the DWBC and North Atlantic Current (e.g. in Fig. 3c and d, where anomalies have same colour as in the Labrador basin) and then, one time frame later, anomalies of the same sign appear in both the western and eastern subtropical basins. This is consistent with the time lag implied by the Bermuda temperature/Labrador basin thickness correlation. The eastern subpolar gyre shows a similar delay, which is consistent with inferred influence times since the 1980s[14,18].

The time-delayed subtropical temperature patterns seem to represent the slow adjustment of the subtropical deep water's advective–diffusive balance to the waxing and waning LSW. As the LSW source thickens, its role in that balance strengthens and this is manifested as an eastwards and southwards erosion of the MOW influence on the subtropical deep water and thus cooler and fresher UNADW. The time required for the advective elements to circulate and mix the LSW into the subtropical basins results in a delayed appearance of the response. When the LSW is thinner than normal, the MOW is able to exert more influence on the advective–diffusive balance, and this appears as a westwards and northwards extension of its warm, salty and thin characteristics.

Understanding the nature of the subtropical temperature response and knowing that subpolar convection has been extreme from 1988 to 1995 prompts us to speculate that the subtropical mid-depths will continue to cool throughout the 1990s and the early 2000s. The cold, fresh and thick signal now invading the subtropics is quite pronounced in the bottom panels of Fig. 3 and will undoubtedly have profound effects on the UNADW properties. The colder, fresher UNADW arrived at Bermuda in August 1996. And its arrival in the DWBC at 26° N was noted by increased chlorofluorocarbon concentrations in 1996 by Miami researchers[19] who have been monitoring this region for about a decade. If the NAO index were to remain persistently high and subpolar convection strong, then the 40-year warming of the subtropical mid-depths would reverse to a substantial cooling. A switch from the high NAO of the 1980s and early 1990s to a persistent low index with weak subpolar convection, however, would again reduce the amount of LSW entering the subtropics and this impending cooling could appear as just another decadal oscillation in the long-term record. Such a switch might be in progress, for the NAO index has been low for two consecutive winters: 1995/96 and 1996/97. □

Received 17 March; accepted 14 October 1997.

1. Deser, C. & Blackmon, M. Surface climate variations over the North Atlantic Ocean during winter: 1900–1989. *J. Clim.* **6,** 1743–1753 (1993).
2. Kushnir, Y. & Held, I. M. Equilibrium atmospheric response to North Atlantic SST anomalies. *J. Clim.* **9,** 1208–1220 (1996).
3. Griffies, S. M. & Bryan, K. A predictability study of simulated North Atlantic multidecadal variability. *Clim. Dyn.* **13**(7/8), 459–487 (1997).
4. Dickson, B. From the Labrador Sea to global change. *Nature* **386,** 649–650 (1997).
5. Sutton, R. T. & Allen, M. R. Decadal predictability of North Atlantic Sea surface temperature and climate. *Nature* **388,** 563–565 (1997).
6. McCartney, M. S. Is the ocean at the helm? *Nature* **388,** 521–522 (1997).
7. Dickson, R., Lazier, J., Meincke, J., Rhines, P. & Swift, J. Long-term coordinated changes in the convective activity of the North Atlantic. *Prog. Oceanogr.* **38,** 241–295 (1996).
8. Bryden, H. L. *et al.* Decadal changes in water mass characteristics at 24° N in the subtropical North Atlantic Ocean. *J. Clim.* **9,** 3162–3186 (1996).
9. Joyce, T. M. & Robbins, P. The long-term hydrographic record at Bermuda. *J. Clim.* **9,** 3121–3131 (1996).
10. Roemmich, D. & Wunsch, C. Apparent changes in the climatic state of the deep North Atlantic Ocean. *Nature* **307,** 447–450 (1984).
11. Levitus, S. Interpentadal variability of temperature and salinity at intermediate depths of the North Atlantic Ocean, 1970–1974 versus 1955–1959. *J. Geophys. Res.* **94,** 6091–6131 (1989).
12. Houghton, R. W. Subsurface quasi-decadal fluctuations in the North Atlantic. *J. Clim.* **9,** 1363–1373 (1996).
13. Lazier, J. R. in *Natural Climate Variability on Decade-to-Century Time Scales of Natural Climate Variability* (ed. Martinson, D. G. *et al.*) 295–302 (National Academy Press, Washington, DC, 1995).
14. Hurrell, J. W. Decadal trends in the North Atlantic Oscillation: regional temperatures and precipitation. *Science* **269,** 676–679 (1995).
15. Dickson, R., Meincke, J., Malmberg, S.-A. & Lee, A. The "Great Salinity Anomaly" in the northern North Atlantic 1968–1982. *Prog. Oceanogr.* **20,** 103–151 (1988).
16. Belkin, I. M., Levitus, S. & Antonov, J. "Great Salinity Anomalies" in the North Atlantic. *Prog. Oceanogr.* (in the press).
17. Talley, L. D. & McCartney, M. S. Distribution and circulation of Labrador Sea Water. *J. Phys. Oceanogr.* **12,** 1189–1205 (1982).
18. Sy, A. *et al.* Surprisingly rapid spreading of newly formed intermediate waters across the North Atlantic Ocean. *Nature* **386,** 675–679 (1997).
19. Molinari, R. *et al.* Fast-track for recently formed Labrador Sea Water: the Deep Western Boundary Current of the North Atlantic Ocean. *Deep-Sea Res.* (submitted).
20. Curry, R. HydroBase: a database and tools for climatologic analysis. (Tech. Rep. WHOI-96-01, Woods Hole Oceanographic Inst, 1996).

Acknowledgements. This work was supported by the Atlantic Climate Change Program of NOAA's Climate and Global Change Program and by the National Science Foundaiton.

Correspondence and requests for materials should be addressed to R.G.C. (e-mail: rcurry@whoi.edu). Data available from flotsam.whoi.edu (128.128.28.187). cd pub/nature/curry_etal.

The generation of plankton patchiness by turbulent stirring

Edward R. Abraham

National Institute of Water and Atmospheric Research, P.O. Box 14-901, Kilbirnie, Wellington, New Zealand

Diffusive processes are often used to represent the formation of spatial patterns in biological systems[1]. Here I show how patchiness may be generated in planktonic ecosystems through non-diffusive advection. Plankton distributions in oceanic surface waters can be characterized by the spectra of concentrations obtained along ship transects. Such spectra are inevitably found to have a power-law form over horizontal scales ranging from 1 to 100 km (ref. 2). Phytoplankton have distributions similar to those of physical quantities such as sea surface temperature, with much less variability at shorter length scales. In contrast, zooplankton density may be almost as variable at short scales as long ones[3]. Distributions of this form are generated in a model of the turbulent stirring of coupled phytoplankton and zooplankton populations. The characteristic spatial patterns of the phytoplankton and zooplankton are a consequence of the timescales of their response to changes in their environment caused by turbulent advection.

The accuracy with which the ensemble-averaged dispersal of passive tracers in turbulent ocean flows may be described by eddy diffusion[4] has encouraged the use of diffusion-based models to study the generation of patchiness in planktonic ecosystems[5–8]. Diffusion causes variability to be transferred from small to large length scales, and so it is widely believed that "in order to be able to form a more finely grained pattern the zooplankton must have some

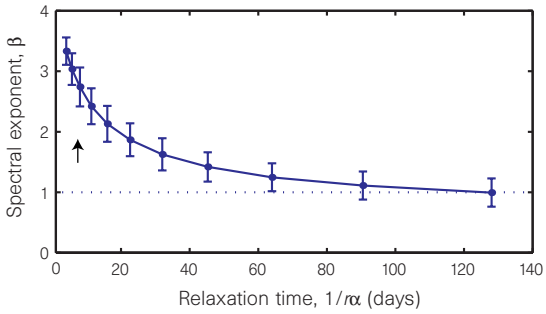

Figure 1 The phytoplankton carrying capacity relaxes towards a smoothly varying background value at a rate α, following equation 1. The power spectrum of a transect, $C(y)$, has the form $\tilde{C}(k) \propto k^{-\beta}$, where the spectral exponent, β, depends on the relaxation rate. Values are mean ± standard deviation of the exponents at the end of a high-resolution model run, calculated from 256 evenly spaced transects by linear regression of $\log(\tilde{C}(k))$ on $\log(k)$. With a relaxation time of $1/r\alpha = 8$ d the spectrum has an exponent $\beta_C = 2.74 \pm 0.32$ (arrow); this value of α is used in the text. The broken line marks the spectral exponent expected for a passive non-reacting tracer.

ability to resist turbulent diffusion"[9]. The long-standing history of this approach[10], and the ease with which diffusion can be incorporated into differential equations, has led to the neglect of the fact that true diffusion within the oceanic surface layer is insignificant at larger than centimetre scales. At horizontal scales of between 1 and 100 km, only ensemble-averaged processes should be represented as diffusive. During any single realization, stirring by a turbulent flow causes variability to be transferred from large to small scales: under the action of turbulent advection a patch of tracer develops fine tendrils and filaments. The fine structure in the zooplankton distributions can then be generated by the transfer of variability from larger scales by stirring over the lifetime of the zooplankton. Models of the evolution of the mixed layer in a quasi-geostrophic flow suggest that at mid-latitudes approximately 10 days is required for the transfer of variance from the size of the largest turbulent features (~100 km) to the scale at which three-dimensional flow becomes important (~1 km)[11]. This is less than the lifetime of larger zooplankton such as copepods, which typically require 25 days to reach adult stages[12]. During their maturation time any large-scale variation in the distribution of juvenile copepods will be stirred down to kilometre lengths.

The theory of turbulent transport has enabled phytoplankton patchiness to be understood in terms of both biological growth and physical advection[13–17], and dimensional analysis suggests that zooplankton–phytoplankton interactions may cause increased small-scale variability[18]. Although these theoretical approaches are remarkably powerful, they are difficult to apply to populations with anything beyond the simplest dynamics. In addition, the lack of a suitable representation of turbulent flow has restricted the direct incorporation of turbulent stirring into models of coupled plankton populations. Here the seeded-eddy model of a two-dimensional non-divergent flow[19] is used to simulate turbulent advection (see Box 1). This model represents the turbulence as a sum of randomly distributed eddies of prescribed form. It is not a fluid-dynamic model, but with a judicious choice of parameters it provides a simple and easily implemented proxy for quasi-geostrophic turbulence. The domain of the model is a periodic square with sides of length L of 256 km. A number of independent, uniformly distributed water parcels are advected within this domain by the seeded-eddy flow. Each parcel carries a phytoplankton population density, P, and an adult zooplankton population density, Z, which represents a copepod species. While very large zooplankton, such as krill, may modify their distributions substantially by swimming[20]. It is assumed here that the modelled zooplankton are truly planktonic, drifting with their respective water parcels.

In addition to these populations, each parcel has an associated carrying capacity, C, the maximum phytoplankton concentration attainable within that parcel in the absence of grazing. This carrying capacity may be assumed to represent the effect of a limiting nutrient, or to represent variations in mixed-layer depth. As a parcel moves through the domain, the carrying capacity continually relaxes towards a zonally varying background value, $C_0(x, y) = [1 - \cos(2\pi y/L)]/2$. This injects spatial variability into the model at the longest possible length scale. At the end of a model run the spatial distributions of the variables are obtained from a Delaunay triangulation of the parcel positions, by linear interpolation onto a regular grid[21].

The dimensionless equations coupling the populations within a parcel are

$$\mathrm{d}C/\mathrm{d}t' = \alpha(C_0 - C) \quad (1)$$

$$\mathrm{d}P/\mathrm{d}t' = P(1 - P/C) - PZ \quad (2)$$

$$\mathrm{d}Z/\mathrm{d}t' = P(t' - \tau)Z(t' - \tau) - \delta Z^2, \quad (3)$$

where α is the relaxation rate of the carrying capacity; $t' = rt$ is the dimensionless time; r is the phytoplankton growth rate, which is chosen to be 0.5 d^{-1}; τ/r represents the time taken for the zooplankton to mature; and δ is the zooplankton mortality. Phytoplankton growth is logistic and grazing is through a simple P–Z term: neither grazing saturation nor a minimum phytoplankton concentration at which grazing occurs are included. With $\tau = 0$ these equations reduce to a set previously used in the discussion of plankton patchiness[5]. In the absence of advection the model, at any position, has a single fixed point, $C = C_0$, $P = \delta C_0/(\delta + C_0)$, $Z = P/\delta$. This fixed point is stable for $\tau = 0$. If $C_0 \leq 1$, $\delta \geq 0.5$, as in these simulations, it remains stable when a non-zero maturation time is included.

The importance of response time for determining spatial structure is seen by comparing the distribution of the carrying capacity for different values of the rate parameter, α. When $1/r\alpha$ becomes larger the carrying capacity adjusts more slowly to the turbulent advection. As a consequence the carrying capacity develops increased fine spatial structure and its spectra become flatter (Fig. 1). With $1/r\alpha = 8$ d, transects of the carrying capacity across

Box 1 The seeded-eddy model of a turbulent flow

In this implementation of the seeded-eddy model, the stream function is represented as a sum of N circular eddies

$$\psi(\mathbf{x}, t) = a \sum_{i=1}^{N} (\pm)_i R_i^2 \mathrm{e}^{-|\mathbf{x} - \mathbf{x}_i(t)|^2/2R_i^2}$$

where R_i and $\mathbf{x}_i = (x_i(t), y_i(t))$ specify the radius and centre position of each eddy, a is an overall calibration constant, and each eddy is included in the sum with a randomly assigned orientation. In these simulations the eddy centres are uniformly distributed over a 256-km square periodic domain, and move with the local velocity

$$\partial \mathbf{x}_i/\partial t = \mathbf{v}(\mathbf{x}_i)$$

where $\mathbf{v} = (-\partial\psi/\partial y, \partial\psi/\partial x)$. The turbulence is assumed to form a cascade between an upper radius, $R_{max} = 64$ km, appropriate for mid-latitude ocean turbulence and a lower radius, R_{min}, the resolution limit of the model velocity field. Within this range the probability density of the radius is taken to be $p(R) \sim R^{-3}$, so the area covered by the eddies within each size interval, $\pi N \int_{R/2}^{R} r^2 p(r) \mathrm{d}r$, is constant. The number of eddies, N, is chosen such that there are expected to be 16 eddies with a radius between 32 and 64 km. The spectra of the transverse and longitudinal velocity autocorrelation, taken from snapshots of the velocity field with $R_{min} = 0.5$ km and $N = 87{,}536$, have an order-of-magnitude range of wavenumber where $E(k) \propto k^{-2.7 \pm 0.3}$, in close agreement with theoretical predictions[29]. Because the energy falls of rapidly at high wavenumber, a high-resolution model with $R_{min} = 4$ km and $N = 1{,}360$ is sufficiently detailed. A low-resolution model, with $R_{min} = R_{max} = 64$ km and $N = 16$, is also used. The overall calibration is set to be $a = 0.14\ \mathrm{d}^{-1}$ by requiring the r.m.s. velocity to be $|\mathbf{v}| \sim 10\ \mathrm{cm\ s}^{-1}$. With these parameters the Lagrangian timescale of the seeded-eddy model is $T_L = 7 \pm 3$ d, the Euclidean timescale is $T_E = 14 \pm 2$ d (both calculated from 16 300-day realizations), and the advective timescale $T_a = R_{max}/|\mathbf{v}| = 7.4$ d, in good comparison with experimentally determined values[30].

When the high-resolution model is used, 131,072 tracer parcels and their associated populations are followed, whereas the low-resolution model runs tracks only 8,192 parcels. Integration of both the biological and the physical components of the model is carried out using a simple finite difference scheme. The time step is restricted by the requirement that the parcels maintain a uniform distribution as they are advected. A time step of 0.1 d was found to be sufficiently small. The populations were initialized at their mean equilibrium values and then followed for 300 d. The model was programmed in FORTRAN and run on a Pentium 166-MHz computer, needing 4 s and 5 min for single low- and high-resolution time steps, respectively.

the model domain have spectra with similar exponents to the spectra of physical quantities such as sea surface temperature[22], so the relaxation rate is set at $\alpha = 0.25$. At large relaxation times the spectral exponent becomes close to 1, the value expected for the spectrum of a passive non-reacting tracer in a two-dimensional turbulent flow[18]. This suggests that the turbulent transfer of variability to smaller scales is adequately represented by the seeded-eddy model.

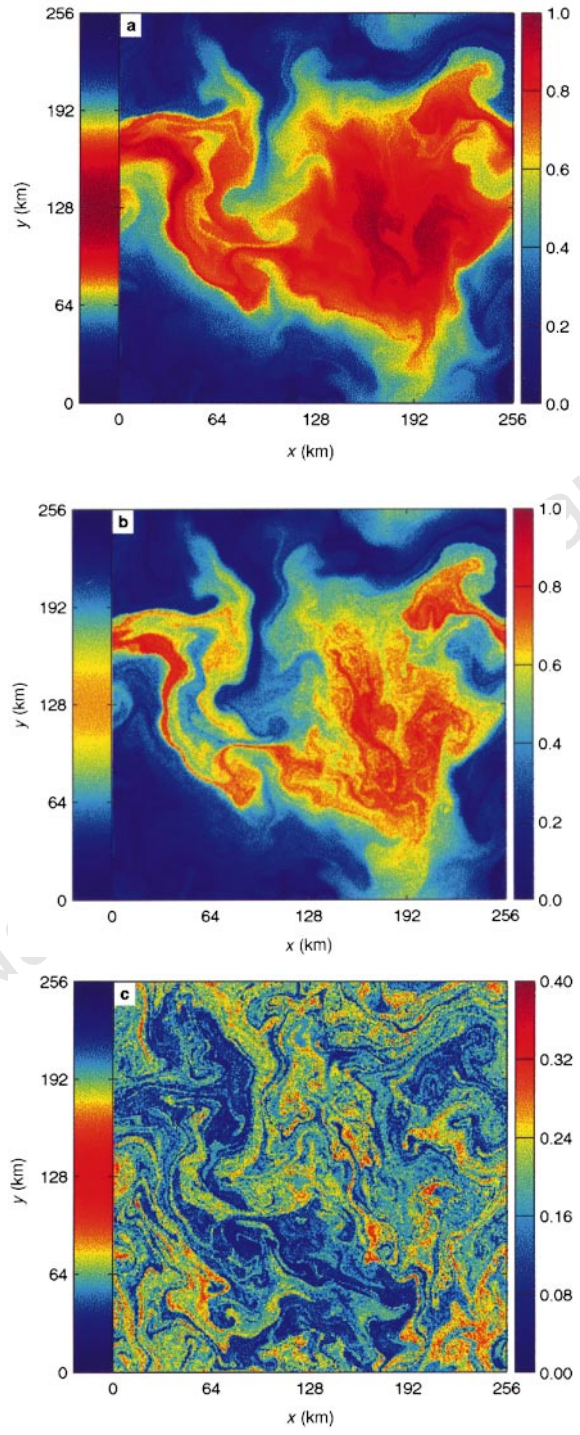

Figure 2 Snapshots at the end of a high-resolution model run. The model follows equations 1–3, with $\tau/r = 25$ d and $\delta = 2$, corresponding to a high P and low Z regime. **a**, Carrying capacity; **b**, phytoplankton, **c**, zooplankton. The strip at the left shows the zonally varying distributions the populations would have in the absence of advection while the bar on the right gives the values associated with the different colours. The distortion due to turbulent stirring is clearly visible.

With the inclusion of advection the continually changing carrying capacity prevents the populations within each parcel from reaching equilibrium. Despite the simplicity of the dynamics, a complex spatial pattern emerges by the end of the model run (Fig. 2). Because of the rapid phytoplankton growth rate, the phytoplankton distribution (Fig. 2b) is similar to the distribution of the carrying capacity (Fig. 2a). In contrast, the zooplankton population (Fig. 2c) has marked fine scale structure. This is clearly seen in a transect through the model domain (Fig. 3a), which simulates the data that would be collected from a ship. There is no coherence between the zooplankton and phytoplankton distributions at the larger length scales, and grazing causes the distributions to be negatively correlated at distances of less than ~10 km. As a consequence, the phytoplankton concentration has a spectrum that is slightly flatter than that of the carrying capacity, but steeper than the zooplankton spectrum (Fig. 3b). These results are in good agreement with observations, which find similar spectra, and which show a similar negative correlation between phytoplankton and zooplankton populations at shorter length scales[2,3,23].

An analysis of the populations obtained by integrating the model with a range of parameter values, and using a simplified representation of the flow, confirms that the relative slopes of these spectra are insensitive to both the precise values of the parameters and the details of the stirring process (Fig. 4). An increasing zooplankton maturation time leads to flatter zooplankton spectra, whereas a

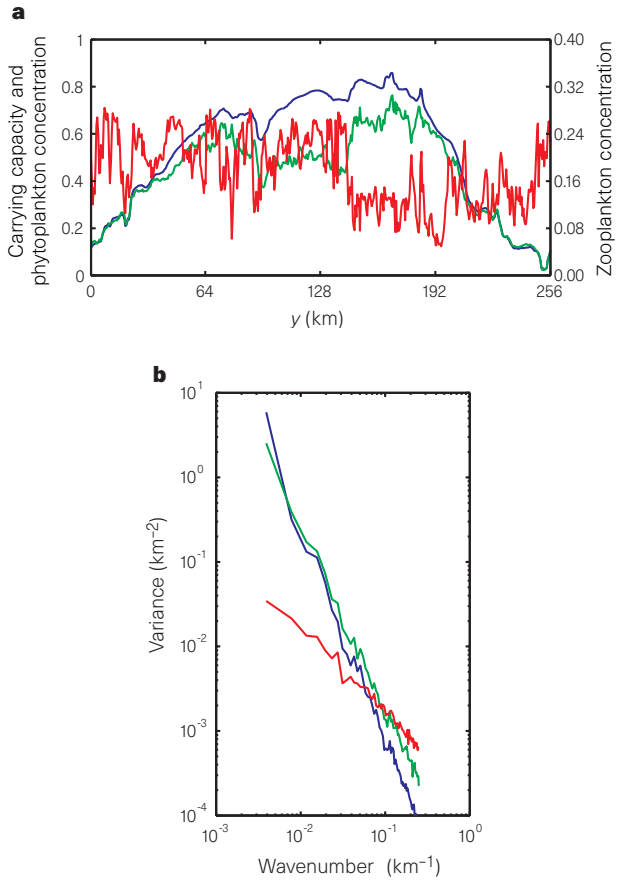

Figure 3 A representative transect and the corresponding spectra. Graphs show carrying capacity (blue), phytoplankton (green) and zooplankton (red). **a**, A transect through the snapshots in Fig. 2 (at $x = 128$ km). The simplicity of the underlying population dynamics is not apparent. **b**, The corresponding spectra have a power-law form over an order of magnitude range. The spectra from 256 evenly spaced transects are averaged to form those shown here. The spectral exponents (mean ± s.d.) of the populations at this time are $\beta_C = 2.5 \pm 0.20$, $\beta_P = 2.1 \pm 0.20$ and $\beta_Z = 1.0 \pm 0.16$.

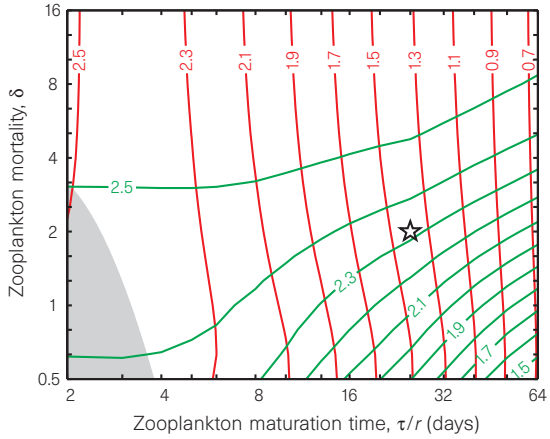

Figure 4 The dependence of the spectral exponents of the phytoplankton (green) and zooplankton (red) populations on the model parameters. The low-resolution model, including only the largest eddies, was run repeatedly with values of δ and τ indicated, but using the same velocity field. The contoured spectral exponents were obtained by averaging the spectra derived from snapshots of the populations at 10-day intervals between 160 and 300 model days. Within the shaded region, $\beta_Z > \beta_P$; elsewhere, the zooplankton have a flatter spectra than the phytoplankton. The star marks the values of the parameters used in Figs 2 and 3.

larger zooplankton mortality leads to phytoplankton distributions with steeper spectra, because of the reduced grazing on the phytoplankton. Because the simplified physics, including only the largest eddies, is less efficient at transferring variability towards smaller length scales, the spectral slopes are steeper than the slopes generated by the model with a full turbulent cascade.

Detailed simulations, incorporating fluid-dynamic models of quasi-geostrophic turbulence, multi-compartment ecosystem dynamics, and seasonal forcing, have been attempted[24]. These simulations find a similar result: that the zooplankton have a flatter spectra than the phytoplankton. Because of the complexity of the processes represented, the source of the fine-scale zooplankton structure in those models is unclear. The power of a simple model is to demonstrate how populations with these different distributions may occur without the need for any mechanism beyond their different response rates to changes in the environment caused by turbulent advection. Although predicting spectral form is a weak test of any theory[25], and the available evidence is perhaps ambiguous (not all data sets show flatly sloped zooplankton spectra[26], and similar results may arise as observational artefacts[27]), this analysis suggests that zooplankton lifetime is an important determinant of their spatial pattern. A new observational sophistication, which enables zooplankton distributions to be tightly related to the physical properties of the surface waters[28], will allow a detailed testing of these relationships. □

Received 3 June; accepted 22 September 1997.

1. Okubo, A. *Biomathematics* Vol. 10, *Diffusion and Ecological Problems: Mathematical Models* (Springer, Berlin, 1980).
2. Mackas, D. L. & Boyd, C. M. Spectral analysis of zooplankton spatial heterogeneity. *Science* **204,** 62–64 (1979).
3. Tsuda, A., Sugisaki, H., Ishimaru, T., Saino, T. & Sato, T. White-noise-like distribution of the oceanic copepod *Neocalanus cristatus* in the subarctic North Pacific. *Mar. Ecol. Prog. Ser.* **97,** 39–46 (1993).
4. Okubo, A. Oceanic diffusion diagrams. *Deep Sea Res.* **18,** 789–802 (1971).
5. Levin, S. A. & Segel, L. A. Hypothesis for origin of plankton patchiness. *Nature* **259,** 659 (1976).
6. Wroblewski, J. S. & O'Brien, J. J. A spatial model of phytoplankton patchiness. *Mar. Biol.* **35,** 161–175 (1976).
7. Steele, J. H. & Henderson, E. W. A simple model for plankton patchiness. *J. Plankton Res.* **14,** 1397–1403 (1992).
8. Malchow, H. Nonequilibrium structures in plankton dynamics. *Ecol. Model.* **75/76,** 123–134 (1994).
9. Parsons, T. R., Takahashi, M. & Hargrave, B. *Biological Oceanographic Processes*, 3rd edn (Pergamon, Oxford, 1984).
10. Kierstead, H. & Slobodkin, L. B. The size of water masses containing plankton blooms. *J. Mar. Res.* **12,** 141–147 (1953).
11. Klein, P. & Hua, B. L. The mesoscale variability of the sea surface temperature: An analytical and numerical model. *J. Mar. Res.* **48,** 729–763 (1990).
12. Kiorboe, T. & Sabatini, M. 1995 Scaling of fecundity, growth and development in marine planktonic copepods. *Mar. Ecol. Prog. Ser.* **120,** 285–298 (1995).
13. Denman, K. L. & Platt, T. The variance spectrum of phytoplankton in a turbulent ocean. *J. Mar. Res.* **34,** 593–601 (1976).
14. Gower, J. F. R., Denman, K. L. & Holyer, R. J. Phytoplankton patchiness indicates the fluctuation spectrum of mesoscale oceanic structure. *Nature* **288,** 157–159 (1980).
15. Lesieur, M. & Sadourny, R. Satellite-sensed turbulent ocean structure. *Nature* **294,** 673 (1981).
16. Bennett, A. F. & Denman, K. L. Phytoplankton patchiness: inferences from particle statistics. *J. Mar. Res.* **43,** 307–335 (1985).
17. Holloway, G. Eddies, waves, circulation and mixing: statistical geofluid mechanics. *Annu. Rev. Fluid Mech.* **18,** 91–147 (1986).
18. Powell, T. M. & Okubo, A. Turbulence, diffusion and patchiness in the sea. *Phil. Trans. R. Soc. Lond. B* **343,** 11–18 (1994).
19. Dyke, P. P. G. & Robertson, T. The simulation of offshore turbulent dispersion using seeded eddies. *Appl. Math. Model.* **9,** 429–433 (1985).
20. Trathan, P. N., Priddle, J., Watkins, J. L., Miller, D. G. M. & Murray, A. W. A. Spatial variabiity of Antarctic krill in relation to mesoscale hydrography. *Mar. Ecol. Prog. Ser.* **98,** 61–71 (1993).
21. Renka, R. J. Triangulation and interpolation at arbitrarily distributed points in the plane. *ACM Trans. Math. Software* **10,** 440–442 (1984).
22. Deschamps, P. Y., Frouin, R. & Wald, L. Satellite determinations of the mesoscale variability of the sea surface temperature. *J. Phys. Oceanogr.* **11,** 864–870 (1981).
23. Mackas, D. L., Denman, K. L. & Abbot, M. R. Plankton patchiness: biology in the physical vernacular. *Bull. Mar. Sci.* **37,** 652–674 (1985).
24. Smith, C. L., Richards, K. J. & Fasham, M. J. R. The impact of mesoscale eddies on plankton dynamics in the upper ocean. *Deep Sea Res. I* **43,** 1807–1832 (1996).
25. Armi, L. & Flament, P. Cautionary remarks on the spectral interpretation of turbulent flows. *J. Geophys. Res.* **C90,** 11779–11782 (1985).
26. Piontkovski, S. A. *et al.* Spatial heterogeneity of the planktonic fields in the upper mixed layer of the open ocean. *Mar. Ecol. Prog. Ser.* **148,** 145–154 (1997).
27. Fasham, M. J. R. in *Spatial Pattern in Plankton Communities* (ed. Steele, J. H.) 131–156 (Plenum, New York, 1978).
28. Gallagher, S. M., Davis, C. S., Epstein, A. W., Solow, A. & Beardsley, R. C. High-resolution observations of plankton spatial distributions correlated with hydrography in the Great South Channel, Geoges Bank. *Deep Sea Res. II* **43,** 1627–1663 (1996).
29. Charney, J. G. Geostrophic turbulence. *J. Atmos. Sci.* **28,** 1087–1095 (1971).
30. Middleton, J. F. Drifter spectra and diffusivities. *J. Mar. Res.* **43,** 37–55 (1985).

Acknowledgements. I thank P. Boyd, P. Sutton, C. Stevens and J. Sharples for critical reading of the draft manuscript, and R. Renka for software made available through the TOMS internet archive that was used to interpolate the Lagrangian variables onto a regular grid.

Correspondence and requests for materials should be addressed to E.A. (e-mail: e.abraham@niwa.cri.nz).

Collinear stimuli regulate visual responses depending on cell's contrast threshold

Uri Polat*, Keiko Mizobe*, Mark W. Pettet, Takuji Kasamatsu & Anthony M. Norcia

The Smith-Kettlewell Eye Research Institute, 2232 Webster Street, San Francisco, California 94115, USA

Neurons in the primary visual cortex are selective for the size, orientation and direction of motion of patterns falling within a restricted region of visual space known as the receptive field[1]. The response to stimuli presented within the receptive field can be facilitated or suppressed by other stimuli falling outside the receptive field which, when presented in isolation, fail to activate the cell[2–8]. Whether this interaction is facilitative[3,4,7,9–12] or suppressive[2,3,5,6,8–14] depends on the relative orientation of pattern elements inside and outside the receptive field. Here we show that neuronal facilitation preferentially occurs when a near-threshold stimulus inside the receptive field is flanked by higher-contrast, collinear elements located in surrounding regions of visual space. Collinear flanks and orthogonally oriented flanks, however, both act to reduce the response to high-contrast stimuli presented within the receptive field. The observed pattern of facilitation and suppression may be the cellular basis for the observation in humans that the detectability of an oriented pattern is enhanced by collinear flanking elements[15–17]. Modulation of neuronal responses by stimuli falling outside their receptive fields may thus represent an early neural mechanism for encoding objects and enhancing their perceptual saliency.

* Present addresses: Institute for Vision Research, Ehad Ha'am 14, Rehovot 76105, Israel (U.P.); Department of Ophthalmology, Kyoto Prefectural University of Medicine, Hirokoji Kawara-machi, Kamigyo-ku, Kyoto 602, Japan (K.M.).